Journal of
Synchrotron Radiation

ISSN 0909-0495

Received 27 February 2009
Accepted 24 August 2009

Phonon spectroscopy at high pressure by inelastic X-ray scattering

Valentina M. Giordano,* Michael Krisch and Giulio Monaco

European Synchrotron Radiation Facility, 6 rue Jules Horowitz, BP 220, 38043 Grenoble Cedex, France. E-mail: valentina.giordano@esrf.fr

The current status of phonon-dispersion studies at high pressure using very high energy resolution inelastic X-ray scattering is discussed. A brief description of the instrumental apparatus is given, together with an illustration of the high-pressure facilities available at the IXS beamlines ID16 and ID28 of the ESRF. Some selected examples of recent studies on crystalline and liquid samples in a diamond anvil cell are then presented.

Keywords: liquid metals and alloys; high-pressure effects in solids and liquids; acoustical properties of liquids.

1. Introduction

Since the first development of high-pressure techniques, the investigation of condensed matter at high density has revealed a number of new phenomena, such as unexpected crystalline structures (McMahon & Nelmes, 2006), the appearance of superconductivity (Struzhkin *et al.*, 2002) and the existence of first-order liquid–liquid transitions (Katayama *et al.*, 2000). Several experimental techniques, coupled with calculations, have been employed in order to unveil the physics behind these phenomena. However, a long-lasting limitation has been the inability to measure phonon dispersion curves at very high density, which can provide information on issues such as interatomic force constants, elastic and thermodynamic properties, deviation from two-body potential approximations and anharmonicity of crystal potentials, thus allowing in particular for a better understanding of the mechanisms driving phase transitions.

For a long time the investigation of the phonon dispersions has traditionally been a prerogative of the inelastic neutron scattering (INS) technique, and the corresponding need of a large amount of samples (several mm^3) has limited the accessible pressure range. For instance, while neutron diffraction measurements have been reported for pressures up to 25 GPa (Ninet *et al.*, 2009), so far, inelastic scattering experiments have been limited to 10 GPa (Klotz *et al.*, 1997; Klotz & Braden, 2000). Only the advent of the high-brilliance third-generation synchrotron radiation sources X-ray beams has enabled inelastic X-ray scattering (IXS) to join in as a complementary technique. The smaller sample size required in this case (10^{-4}–10^{-5} mm^3), together with a beam size of the order of 100 μm, has made IXS the ideal tool for the investigation of the dynamics of condensed matter under extreme thermodynamic conditions. This potential had already been pointed out by Burkel in his review on phonon measurements by IXS (Burkel, 2000) and since then high-pressure applications have been continuously growing in number.

Two other, but not less important, aspects of complementarity of IXS with respect to INS are (i) the possibility to address samples which cannot be investigated by INS because of their high absorption or incoherent cross section for neutrons, and (ii) the absence of any kinematic restriction. Indeed, when the probe is a neutron beam, the dependence of the exchanged momentum Q on both the scattering geometry and the exchanged energy E imposes that the accessible dynamical range is limited, so that excitations of high energy cannot be measured at very low Q. On the contrary, the exchanged momentum in an X-ray experiment is in a very good approximation determined only by the scattering geometry, and the accessible dynamical range is virtually infinite. This difference is not important when single crystals are investigated, as the phonon dispersion curves can be reconstructed by using the information collected in several Brillouin zones. On the contrary, the limitations intrinsic to INS strongly affect the investigation of disordered samples, such as liquids and glasses, for which collective excitations can be detected only in a limited range of small Q. Similar considerations apply to polycrystalline materials, for which only access to small Q values allows for the determination of the orientation-averaged acoustic phonon dispersion curve.

In this paper we will present the status of IXS applications at high pressure. In §2 we will give an overview of the experimental set-up used in these cases, followed by some examples of experiments performed using a diamond anvil cell in §3.

2. Experimental

2.1. IXS set-up

We will briefly describe here the experimental set-ups used for IXS experiments at the ID16 and ID28 beamlines of the ESRF. A thorough illustration of the underlying optical principles is reported by Sette *et al.* (1996).

It is worth noting that the late advent of this technique is due to the formidable experimental challenge that it represents. Indeed, as the X-ray energy usually ranges between 10 and 30 keV, the resolving power required to measure inelastic excitations of a few meV is at least $\Delta E/E = 10^{-7}$, and the experimental set-ups leading to such a high resolution inevitably strongly reduce the incoming photon flux. Only the advent of third-generation synchrotron radiation sources with their high brilliance has made it possible to realise schemes allowing for an energy resolution as high as 1.3 meV.

The IXS instrument is based on a triple-axis spectrometer. The first axis is at the main monochromator, which selects the incoming energy; the second is at the sample goniometer, and fixes the momentum transfer; and the third is at the analyser crystal, which defines the final photon energy. A sketch of the beamline set-up is given in Fig. 1. The X-ray source consists of three undulators, located on a 5 m straight section (http://www.esrf.fr/UsersAndScience/Experiments/HRRS/ID16), which produce a highly collimated beam [40 (H) × 20 (V) μrad FWHM], which is pre-monochromated by a double-crystal silicon monochromator, operating at the [111] reflection, to $\Delta E/E = 1 \times 10^{-4}$. Successively, the beam impinges on the high-resolution backscattering monochromator, which consists of an asymmetrically cut silicon crystal operating at a Bragg angle of 89.98° using a [*hhh*] reflection and diffracting in the vertical plane. This extreme backscattering geometry is required in order to minimize the geometrical contributions to the total energy resolution and insures an intrinsic spectral angular acceptance (Darwin width) larger than the X-ray beam divergence, so that all the photons within the desired energy bandwidth are diffracted. The goal of an energy resolution as high as $\Delta E/E = 10^{-7}$–10^{-8} requires the use of a perfect crystal for the monochromator and of high-order Bragg reflections. A specific Si (*h*,*h*,*h*) backscattering reflection is chosen by tuning the pre-monochromator to the correct

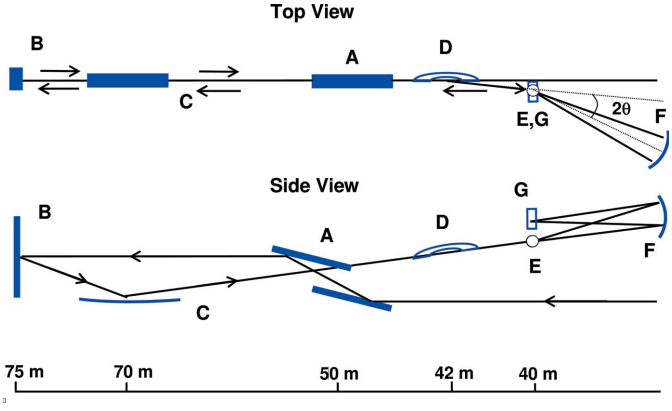

Figure 1
Sketch of the experimental set-up at the ID16 and ID28 beamlines of the ESRF. A: double Si(1,1,1) monochromator, providing an energy resolution $\Delta E/E = 10^{-4}$. B: high-resolution backscattering monochromator, providing an energy resolution $\Delta E/E = 10^{-7}$–10^{-8}. C: Pt-coated toroidal mirror for horizontal and vertical focusing. D: multilayer mirror for horizontal focusing, used for high-pressure experiments. E: sample. F: spherical perfect silicon crystal analyzer operated in Rowland geometry. G: Peltier-cooled silicon diode.

Table 1
Characteristics of the ESRF IXS spectrometers for the most typically used reflections Si (*h*,*h*,*h*).

E is the incident energy and ΔE is the total instrumental energy resolution. $Q_n - Q_m$ is the *Q*-spacing between the analyzers, ΔQ is the typical *Q* resolution in the horizontal scattering plane. The photon flux has been measured at the sample position and is here reported for a representative ring current of 100 mA. The better performance of the Si (12,12,12) with respect to the Si (11,11,11) is due to the use, in the former case, of two 26 mm-gap undulators, optimized for high energy. The use of the multilayer mirror leads to an intensity loss of 30% with respect to the reported values.

h	*E* (keV)	ΔE (meV)	$Q_n - Q_m$	ΔQ	Flux [photons s^{-1} (100 mA)$^{-1}$]
8	15.817	6	1.07	0.25	4×10^{10}
9	17.793	3	1.2	0.28	2×10^{10}
11	21.747	1.5	1.47	0.34	4×10^{9}
12	23.724	1.35	1.6	0.37	5×10^{9}

energy. The higher the index *h* the better the energy resolution, but the lower the beam intensity onto the sample. A summary of the typical reflections currently used is reported in Table 1.

The highly monochromated beam with meV resolution then impinges onto a Pt-coated toroidal mirror, which provides a focal size of 250 (H) × 60 (V) μm FWHM at the sample position. For high-pressure experiments, a cylindrical side part of that mirror is used for vertical focusing, while a horizontal focus of 30 μm is obtained by means of a multilayer mirror with a lattice spacing gradient installed 2 m before the sample (Morawe *et al.*, 1999).

The photons scattered from the sample are energy-analyzed by spherical perfect silicon crystal analyzers, housed in a vacuum chamber mounted at 6.5 m from the sample on a spectrometer arm. Its rotation in the horizontal plane determines the exchanged momentum *Q*. The analyzers are operated in Rowland geometry, and at the same (*h*,*h*,*h*) reflection order and Bragg angle as the monochromator. The energy-analyzed intensity diffracted by the analyzers is then collected by Peltier-cooled silicon diodes.

Both beamlines are equipped with nine analyzers with a constant angular offset of about 0.75°, each one diffracting onto a different silicon diode. This allows for the simultaneous collection of spectra at nine different values of the exchanged momentum *Q*.

The IXS scan is usually performed in a constant *Q* mode, by changing the energy difference between monochromator and analyzer. However, as a consequence of the extreme backscattering geometry, this cannot be done by modifying the Bragg angle of one of the two crystals. The chosen solution consists of changing the temperature *T* of the monochromator. The corresponding relative variation in the lattice constant, $\Delta d/d = \alpha(T)\Delta T$, induces a relative energy variation $\Delta E/E = -\Delta d/d$ at a given Bragg angle. In order to change the energy in the meV range, given that $\alpha \simeq 2.58 \times 10^{-6}\ \mathrm{K}^{-1}$ at room temperature, a temperature control of both monochromator and analyzer crystals in the mK regime is required. The correct conversion from temperature to energy scale was checked by comparison with the well established dispersion of long-

itudinal acoustic and optical phonons in a diamond single crystal and the Raman-active molecular vibration mode in liquid nitrogen (Verbeni *et al.*, 2008).

2.2. IXS at high pressure

The first high-pressure IXS experiments at the ESRF date from the late 1990s, using both large-volume cells of piston-cylinder type (maximum pressure 5 kbar) (LVC) (Mermet *et al.*, 1998; Cunsolo *et al.*, 1999) and diamond anvil cells (DAC) (Krisch *et al.*, 1997; Occelli *et al.*, 2001). Since then, the quality of the spectra has significantly improved, allowing for shorter counting times, thanks to the higher source brilliance and to a continuous improvement of the spectrometers in terms of efficiency, resolution and focusing schemes. This has stimulated an always increasing use of the DAC in order to access higher pressures, though the technical difficulties to be faced are not negligible. An inspection of Table 1 clearly reveals the need of finding a compromise between the desired energy resolution and the required photon flux. Indeed, a high flux is to be preferred whenever the sample thickness cannot be optimized for the IXS experiment, *i.e.* it cannot be chosen equal to the absorption length $t_\mu = 1/\mu$, where μ is the photoelectric absorption coefficient at the selected photon energy. This is often the case in high-pressure experiments, where the typical sample thickness in a DAC is about 40–80 µm, which meets the optimization criterium for high-Z compounds but can be several orders of magnitude smaller than that for light samples: for example, the attenuation length of water at 21.7 keV is 17.2 mm. This is the reason why the high-pressure experiments with a DAC performed so far have mostly been done using the Si (9,9,9) reflection. This is indeed the case for the selected examples reported in the following section, except for the first one, where the Si (8,8,8) reflection was used instead.

Both beamlines ID16 and ID28 are equipped with a vacuum chamber for experiments in a DAC at room and high temperature. A sketch of the one designed for ID16, able to host membrane-driven DACs with an external diameter of 50 and 60 mm, is given in Fig. 2. Besides being necessary to prevent the diamond oxidation for high-temperature operation, a vacuum chamber is also very useful in IXS experiments on disordered or polycrystalline systems, where small Q are of interest, in order to suppress the small angle signal owing to scattering from air.

The chamber provides an easy optical access in order to measure on-line the sample pressure by laser-exciting and measuring the fluorescence line of a gauge placed in the sample chamber (Datchi *et al.*, 1997; Bell & Mao, 1986). Pressure can also be estimated by means of the equation of state of some calibrant thanks to the availability of a MAR CCD or a custom-designed CCD camera allowing for the detection of the diffraction pattern.

An external resistive heater is wrapped around the cell for high-temperature operation, and a clamping system is used to provide a good thermal contact; two thermal screens are also present, to reduce the thermal losses owing to irradiation. This

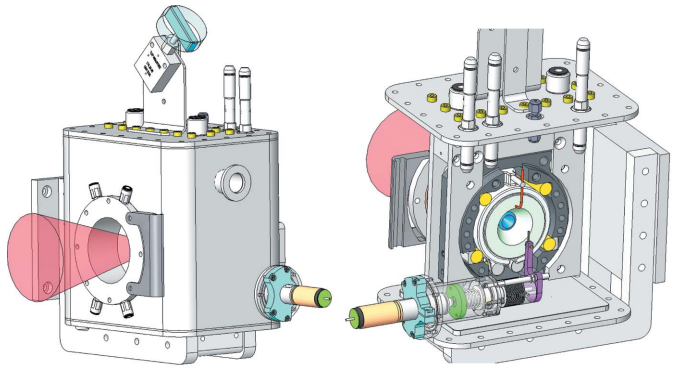

(*a*) (*b*)

Figure 2
(*a*) External view of the vacuum chamber for high-pressure high-temperature experiments. The cone shows the optical opening for pressure measurements. (*b*) A view of the internal mounting. The cell is hosted in a cylindrical heater clamped around it to achieve a good thermal contact. Two thermal screens are mounted on the front and back side of the cell to reduce thermal irradiation but they are not shown here. The beamstop, placed inside the chamber, avoids any possible spurious scattering contribution from the exit window.

set-up provides temperatures as high as 950 K, which are monitored by means of thermocouples in contact with both the outer part of the cell and the diamonds. A motorized beamstop internal to the chamber avoids spurious scattering from the exit window.

Experiments with the use of an internal rather than external resistive heater have also been performed with a different cell and a chamber designed for this purpose (Antonangeli *et al.*, 2008). This chamber allows for measurements at large scattering angles, and is equipped with an internal motorized rotator for the precise alignment of single crystals.

3. Selected examples

We have selected two examples representative of the latest achievements concerning IXS measurements on crystalline samples, while we briefly go through all the existing experiments on liquids, which are limited to only three reports on water (Krisch *et al.*, 2002), fluid oxygen (Gorelli *et al.*, 2006) and liquid caesium (Giordano & Monaco, 2009).

3.1. Phonon branches at high pressure

Many experiments on crystalline samples at high pressure have been performed in the last decade, comprising the study of elemental solids, minerals and strongly correlated electron systems. Several of them aimed to clarify the properties of materials of geophysical interest at thermodynamic conditions comparable with those in the interior of the Earth. This would allow for better constraining models on the composition of the Earth's core, as well as of planets.

A good example of the relevance of dynamic data in this context has been recently given by Badro *et al.* (2007). In this work the authors draw some conclusions on the composition of the Earth's core, by investigating at high pressure the effect on the speed of sound of the addition of light elements to iron.

In fact, it is well known that the main constituent of the Earth's core is iron. It is, however, not straightforward to determine which light elements could be present in addition to it, and in what proportion. With the aim of constraining core composition models, the authors measured the dispersion of the longitudinal acoustic phonons of polycrystalline samples of FeO, FeSi, FeS and FeS_2 at high pressure, and deduced the sample density from the diffraction pattern which was simultaneously collected. The availability of both velocity and density data (Fig. 3) allowed them to reconstruct the composition–velocity and composition–density profiles of terrestrial solid core models constituted of iron and one light element. By comparing their results with seismic models, they could finally propose an average composition for the Earth's core, made of iron and a few weight percent of silicon and traces of oxygen, with the amount of oxygen increasing in the outer core with respect to the inner core.

It is important to mention that the extraction of the sound velocity from polycrystalline IXS data relies on the precise determination of the initial slope of the orientation-averaged longitudinal acoustic phonon branch. Particular care has to be taken in the case of strongly anisotropic systems, and if texture needs to be included (Bosak *et al.*, 2007).

The possibility of measuring phonon dispersion and elastic properties at extreme conditions by means of IXS is also interesting for the investigation of novel structures and materials, for example to understand the driving mechanisms of phase transitions and the interatomic interactions characterizing them. One of the most striking recent reports in this respect is the discovery of surprisingly complex structures in simple metals at high pressure, such as incommensurately modulated structures or incommensurate guest–host composite structures (McMahon & Nelmes, 2006). Besides the structural characterization of all these phases, the measurement of other physical properties is needed for a deeper understanding, for example by giving information on the interaction between atoms of the same kind playing a different role in the structure, like guest and host atoms. Recently, Loa *et al.* (2007) have investigated the phonon dispersion relation of the incommensurate guest–host phase of rubidium, Rb-IV, stable between 16 and 20 GPa. In this phase the guest atoms are arranged along unidimensional chains, as shown in the inset of Fig. 4, and the question arises as to whether the host structure and the chains are strongly interacting or not. The authors measured the longitudinal acoustic phonon dispersion of a single crystal of Rb-IV as a function of pressure along the direction of the chains, and could observe two well defined longitudinal acoustic phonon branches, which they ascribed to separate excitations from the two sublattices (Fig. 4), thus supporting a weak host–guest interaction. Furthermore, the density dependence of the sound velocity of the chains could be very well reproduced with the simple model of a monoatomic chain; the Rb chains in this exotic phase can thus be seen as the physical realisation of this model.

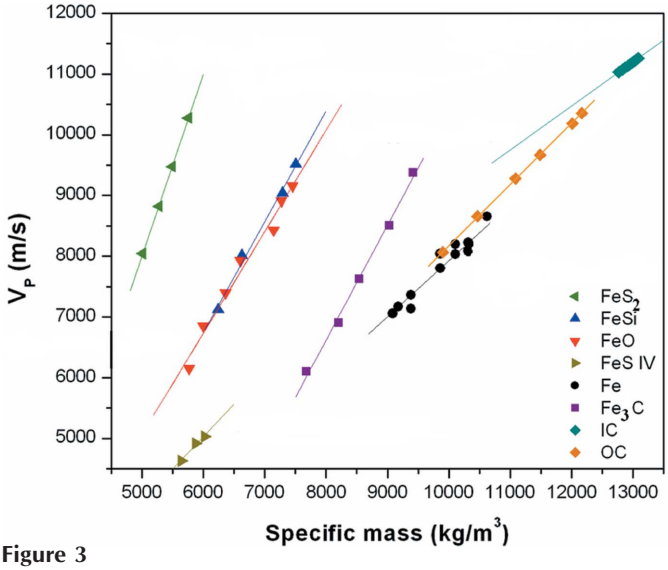

Figure 3
Compressional (P-wave) wave velocities v_P in Fe, FeS, FeO, FeS_2 and FeSi as a function of density ρ. Seismic velocity profiles from the radial PREM model for the inner and outer core (IC and OC, respectively) are also reported. (Adapted from Badro *et al.*, 2007.)

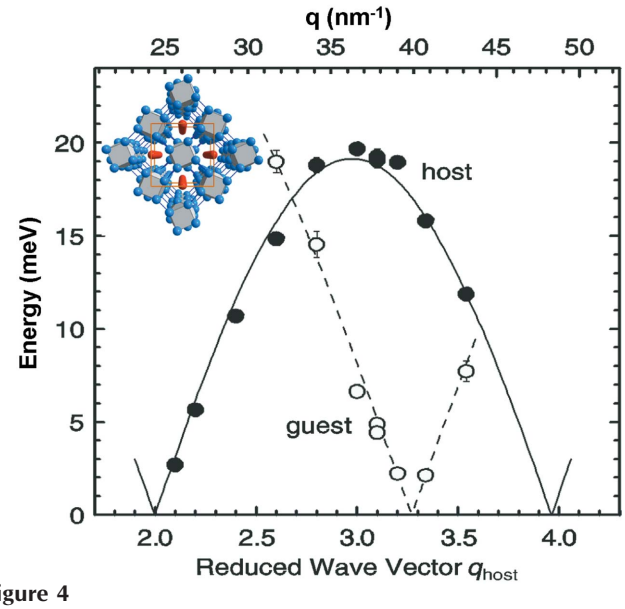

Figure 4
Dispersion relations of longitudinal acoustic excitations in Rb-IV at 17.3 GPa. The reduced wavevector q (parallel to the chains) refers to the reciprocal lattice of the host. The two branches are attributed to lattice excitations of the host (solid symbols) and the guest (open symbols), respectively. The inset shows the structure of Rb-IV. (Adapted from Loa *et al.*, 2007.)

3.2. High-frequency dynamics of liquid systems at high pressure

The physics of liquids has proved to be a rich and largely unexplored field, and high-pressure studies allow for the investigation of structural and electronic properties over a large density range. One of the most intriguing questions concerns the physical origin of the observed dispersion curves of acoustic-like excitations and their relation to the corresponding solid phases. This is even more interesting when a liquid–liquid first-order transition (LLT) is concerned. Since the first observation of such a transition in a pure isotropic

system, namely liquid phosphorus (Katayama *et al.*, 2000), liquid–liquid transitions have been observed or predicted in a continuously growing number of systems, both molecular and monoatomic (McMillan *et al.*, 2007).

The relevance of INS or IXS techniques for the investigation of liquids was recognized a long time ago, as it gives access to the microscopic (*i.e.* atomic) dynamics of the system (Balucani & Zoppi, 1994). It is well known that liquids are able to sustain collective excitations reminiscent of phonons in solids, and that inelastic techniques allow for the measurement of the acoustic dispersion $\omega(Q)$. The specific interest of IXS or INS with respect to low-frequency techniques such as ultrasound (US) or Brillouin light spectroscopy (BLS) lies in the Q and ω range involved. Indeed, the Q range explored in an IXS experiment, $Q \simeq 1$–$20\ \mathrm{nm}^{-1}$, corresponds to typical interparticle distances, while the one measured in US and BLS experiments is macroscopic, being $q \leq 0.01\ \mathrm{nm}^{-1}$. Moreover, the frequency window covered by IXS is in the THz range; as a consequence, the dynamics is affected by relaxation processes with characteristic times of the order of picoseconds. This is the case for the relaxation owing to structural rearrangements, intimately related to the nearest-neighbours interaction, which causes the sound velocity to be frequency-dependent and increase from the low-frequency adiabatic value v_0 towards the infinite frequency limit v_∞ ('positive dispersion'). The investigation of the high-frequency dynamics as a function of density can thus give an insight into the microscopic transformations, structural and dynamical, that the liquid undergoes. While for a long time this has been done mainly by changing the temperature, the ability to control pressure offers the unique chance of exploring a much larger density range.

The first experiment on a liquid sample in a DAC was performed by Krisch *et al.* (2002) on water. Despite its paramount importance, water is a system still not fully understood. This explains the continuous experimental and theoretical effort, focusing in particular on the role of the hydrogen-bonding network. As the structural rearrangements in water are controlled by the hydrogen bonds, the study of its high-frequency dynamics can provide important information. In the referred to IXS experiment, the use of both a large-volume cell and a DAC allowed the authors to follow the dynamics of water in a density range from 1 to 1.4 g cm^{-3}. Studying the density behaviour of both the infinite and low-frequency sound velocities (Fig. 5), the authors could conclude that the role of the hydrogen-bond network becomes less and less relevant with increasing density, so that dense water behaves basically like a simple liquid.

The investigation of the density behaviour of the infinite-frequency sound velocity in liquids exhibiting a LLT is also interesting, as this quantity can provide information on the transition through its dependence not only on the local order but also on the details of the interparticle potential. An example of a system worth investigating in this context is liquid caesium. As a liquid alkali metal, it belongs to the class of simple liquids which has been constantly addressed in order to test microscopic theories of liquids. Their structure and

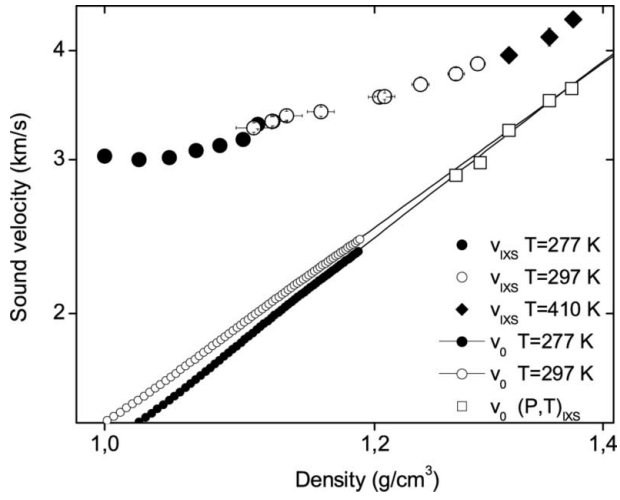

Figure 5
Density behaviour of the sound velocity as measured in liquid water at high pressure. The high-frequency sound velocity v_∞ (full circles: LVC; open circles and full diamonds: DAC) shows clearly a different behaviour with respect to that of the low-frequency. The density evolution of v_0 at 277 and 297 K was obtained from the water equation of state. The solid lines show their extrapolation to higher densities where water would freeze. The squares indicate the value of v_0 at the thermodynamic conditions of the IXS experiment. (Adapted from Krisch *et al.*, 2002.)

dynamics at the room-pressure melting point, as well as at high temperature, have been largely investigated (Balucani & Zoppi, 1994). However, a test of the validity of their theoretical description at high density, where the core–core repulsion becomes more relevant, was still missing until recently (Giordano & Monaco, 2009). More interestingly, caesium exhibits a LLT at a rather low pressure, 3.8 GPa at 500 K, which is electronically driven, and related to a pressure-induced *s*–*d* hybridization (Falconi *et al.*, 2005; Falconi & Ackland, 2006). Giordano & Monaco (2009) reported an IXS experiment on liquid caesium at 500 K between 0.3 and 5 GPa, where the evolution of the acoustic dispersion is followed up to a volume contraction as large as 50% (Fig. 6). It was found

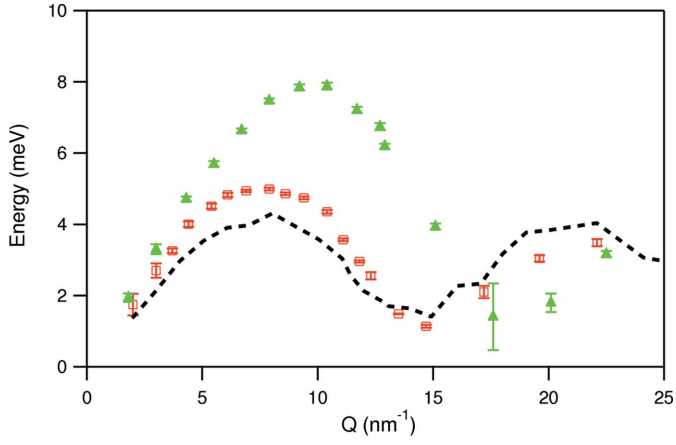

Figure 6
Dispersion curve of the acoustic excitations of liquid caesium at 500 K and 0.3 (squares) and 5 GPa (triangles). Neutron scattering results at the room-pressure melting point are also reported (dashed line) (Bodenstein *et al.*, 1992). (Adapted from Giordano & Monaco, 2009.)

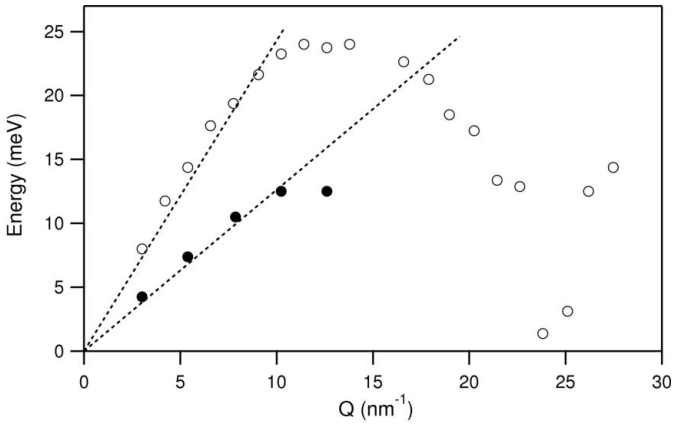

Figure 7
Dispersion relation of supercritical oxygen at 300 K and 0.88 (filled circles) and 5.35 GPa (open circles). Dotted lines are the adiabatic sound velocities as determined by low-frequency techniques. (Adapted from Gorelli *et al.*, 2006.)

that the shape of the acoustic dispersion is unaffected by the density change and even by the LLT. Moreover, the dispersion curves are found to scale on a single master curve, which turns out to be followed also by all the data available in the literature for liquid alkali metals. This was explained as being due to the existence of a unique interatomic potential common to all the alkali metals in very different thermodynamic conditions.

The study of the infinite-frequency sound velocity determined by IXS is also at the focus of the experiment on fluid oxygen at high pressure reported by Gorelli *et al.* (2006). The motivation of this work was to understand whether a fluid under deep supercritical conditions (*i.e.* $P \gg P_c$ and $T \gg T_c$ where P_c and T_c are the pressure and temperature at the critical point) exhibits a gas-like or a liquid-like dynamical behaviour. The two cases are quite different, as in the former the structural relaxation will be very weak or absent, depending on the distance from the extrapolation of the liquid to gas transition line, while in the latter it will be characterized by a non-negligible strength. In order to address this issue, the high-frequency dynamics of fluid oxygen were investigated at room temperature up to 5.35 GPa, focusing especially on the presence of a positive dispersion of the sound velocity as the signature of a liquid-like dynamical behaviour. The fact that oxygen exhibits a positive dispersion as large as 20% at pressures and temperatures well above the critical point (Fig. 7) was interpreted as the demonstration that in the explored thermodynamic conditions the fluid behaves like a liquid. The authors could then conclude that the extrapolation of the Widom line marks the crossover between a liquid-like and a gas-like region (Gorelli *et al.*, 2006).

4. Conclusions

We have presented in this work a brief review of inelastic X-ray scattering with very high energy resolution applied to high-pressure studies. The recent continuous improvement of synchrotron radiation sources and X-ray focusing optics has indeed made it possible to measure IXS spectra on samples in DACs, thus giving access to new and exciting physics.

Owing to the abundance of experiments on high-pressure crystalline samples, we have chosen to refer to only two quite recent reports, one on polycrystals and the other on a single crystal, in order to give a flavour of the physics which can be unveiled by using phonon dispersion data. In particular, the two examples are representative of the contribution of IXS to the current main research directions in the high-pressure field, *i.e.* the understanding of the Earth's interior and the discovery, characterization and understanding of novel structures and materials.

On the contrary, the high-frequency dynamics of liquids at high pressure represent a research field still largely unexplored, not only due to technical difficulties but also to the non-trivial interpretation of the data. This explains the small number of experiments reported (so far), which we have briefly described here. In all these cases, IXS proves to be an efficient tool for investigating the microscopic changes that the liquid undergoes at high density, which is of clear interest in particular for the understanding of liquid–liquid phase transitions.

In the last decade the high-pressure activity on the IXS beamlines of the synchrotron centres worldwide has significantly increased and this tendency is expected to carry on as the experimental set-ups are continuously improving. Furthermore, the recently established possibility of performing both high-pressure and high-temperature experiments will certainly open new avenues both for geophysics and for fundamental physics research.

The authors wish to acknowledge C. Henriquet and D. Gambetti for their technical support and engagement in developing the high-pressure environment on ID16 and ID28. J. Jacobs and D. Gibson are thanked for their continuous support and expert advice. The authors are also grateful to the users from the high-pressure community for fruitful discussions.

References

Antonangeli, D., Krisch, M., Farber, D. L., Ruddle, D. G. & Fiquet, G. (2008). *Phys. Rev. Lett.* **100**, 085501.
Badro, J., Fiquet, G., Guyot, F., Gregoryanz, E., Occelli, F., Antonangeli, D. & D'Astuto, M. (2007). *Earth Planet. Sci. Lett.* **254**, 233–238.
Balucani, U. & Zoppi, M. (1994). *Dynamics of the Liquid State.* Oxford: Clarendon Press.
Bell, P. M. & Mao, H. K. (1986). *Shock Waves in Condensed Matter*, pp. 125–130. New York: Plenum.
Bodensteiner, T., Morkel, C., Glaser, W. & Dorner, B. (1992). *Phys. Rev. A*, **45**, 5709–5720.
Bosak, A., Krisch, M., Fischer, I., Huotari, S. & Monaco, G. (2007). *Phys. Rev. B*, **75**, 064106.
Burkel, E. (2000). *Rep. Prog. Phys.* **63**, 171–232.
Cunsolo, A., Ruocco, G., Sette, F., Masciovecchio, C., Mermet, A., Monaco, G., Sampoli, M. & Verbeni, R. (1999). *Phys. Rev. Lett.* **82**, 775–778.
Datchi, F., LeToullec, R. & Loubeyre, P. (1997). *J. Appl. Phys.* **81**, 3333–3339.

Falconi, S. & Ackland, G. J. (2006). *Phys. Rev. B*, **73**, 184204.
Falconi, S., Lundegaard, L. F., Hejny, C. & McMahon, M. I. (2005). *Phys. Rev. Lett.* **94**, 125507.
Giordano, V. M. & Monaco, G. (2009). *Phys. Rev. B*, **79**, 020201(R).
Gorelli, F., Santoro, M., Scopigno, T., Krisch, M. & Ruocco, G. (2006). *Phys. Rev. Lett.* **97**, 245702.
Katayama, Y., Mizutan, T., Utsumi, W., Shimomura, O., Yamakata, M. & Funakoshi, K. (2000). *Nature (London)*, **403**, 170–173.
Klotz, S., Besson, J. M., Braden, M., Karch, K., Pavone, P., Strauch, D. & Marshall, W. G. (1997). *Phys. Rev. Lett.* **79**, 1313–1316.
Klotz, S. & Braden, M. (2000). *Phys. Rev. Lett.* **85**, 3209–3212.
Krisch, M., Loubeyre, P., Ruocco, G., Sette, F., Cunsolo, A., D'Astuto, M., LeToullec, R., Lorenzen, M., Mermet, A., Monaco, G. & Verbeni, R. (2002). *Phys. Rev. Lett.* **89**, 125502.
Krisch, M., Mermet, A., Miguel, A. S., Sette, F., Masciovecchio, C., Ruocco, G. & Verbeni, R. (1997). *Phys. Rev. B*, **56**, 8691–8694.
Loa, I., Lundegaard, L. F., McMahon, M. I., Evans, S. R., Bossak, A. & Krisch, M. (2007). *Phys. Rev. Lett.* **99**, 035501.
McMahon, M. I. & Nelmes, R. J. (2006). *Chem. Soc. Rev.* **35**, 943–963.
McMillan, P. F., Wilson, M., Wilding, M. C., Daisenberger, D., Mezouar, M. & Greaves, G. N. (2007). *J. Phys Condens. Matter*, **19**, 415101.
Mermet, A., Cunsolo, A., Duval, E., Krisch, M., Masciovecchio, C., Perghem, S., Ruocco, G., Sette, F., Verbeni, R. & Viliani, G. (1998). *Phys. Rev. Lett.* **80**, 4205–4209.
Morawe, C., Pecci, P., Peffen, J.-C. & Ziegler, E. (1999). *Rev. Sci. Instrum.* **70**, 3227–3232.
Ninet, S., Datchi, F., Klotz, S., Hamel, G., Loveday, J. S. & Nelmes, R. J. (2009). *Phys. Rev. B*, **79**, 100101(R).
Occelli, F., Krisch, M., Loubeyre, P., Sette, F., Toullec, R. L., Masciovecchio, C. & Rueff, J.-P. (2001). *Phys. Rev. B*, **63**, 224306.
Sette, F., Ruocco, G., Krisch, M., Masciovecchio, C. & Verbeni, R. (1996). *Phys. Scr.* T**66**, 48–56.
Struzhkin, V. V., Eremets, M. I., Gan, W., Mao, H. K. & Hemley, R. J. (2002). *Science*, **298**, 1213–1215.
Verbeni, R., D'Astuto, M., Krisch, M., Lorenzen, M., Mermet, A., Monaco, G., Requardt, H. & Sette, F. (2008). *Rev. Sci. Instrum.* **79**, 083902.